

1 **Programmed cell death in diazotrophs and the fate of organic**
2 **matter in the western tropical South Pacific Ocean during the**
3 **OUTPACE cruise**

4

5 Dina Spungin¹, Natalia Belkin¹, Rachel A. Foster², Marcus Stenegren², Andrea Caputo²,
6 Mireille Pujo-Pay³, Nathalie Leblond⁴, Cecile Dupouy⁴, Sophie Bonnet⁵, Ilana Berman-
7 Frank^{1*}

8

9 ¹: The Mina and Everard Goodman Faculty of Life Sciences, Bar-Ilan University, Ramat-Gan, Israel.

10 ²: Stockholm University, Department of Ecology, Environment and Plant Sciences. Stockholm, Sweden.

11 ³: Laboratoire d'Océanographie Microbienne – UMR 7321, CNRS - Sorbonne Universités, UPMC Univ Paris 06,
12 Observatoire Océanologique, 66650 Banyuls-sur-mer, France.

13 ⁴: Observatoire Océanologique de Villefranche, Laboratoire d'Océanographie de Villefranche, UMR 7093,
14 Villefranche-sur-mer, France.

15 ⁵: Aix-Marseille Univ., Univ. Toulon, CNRS/INSU, IRD, UM 110, Mediterranean Institute of Oceanography
16 (MIO) UM 110, 13288, Noumea, New Caledonia.

17 *Current address: Leon H. Charney School of Marine Sciences, University of Haifa, Mt. Carmel,
18 Haifa 3498838, Israel

19

20 *Correspondence to:* Ilana Berman-Frank (iberman2@univ.haifa.ac.il)

21

22

23

24

25

26

27

28

29 **Abstract**

30 The fate of diazotroph (N₂ fixers) derived carbon (C) and nitrogen (N) and their contribution to vertical
31 export of C and N in the Western Tropical South Pacific Ocean was studied during the OUTPACE
32 experiment (Oligotrophy to UItra-oligotrophy PACific Experiment). Our specific objective during
33 OUTPACE was to determine whether autocatalytic programmed cell death (PCD), occurring in some
34 diazotrophs, is an important mechanism affecting diazotroph mortality and a factor regulating the
35 vertical flux of organic matter and thus the fate of the blooms. We sampled at three long duration (LD)
36 stations of 5 days each (LDA, LDB, and LDC) where drifting sediment traps were deployed at 150, 325
37 and 500 m depth. LDA and LDB were characterized by high chlorophyll *a* (Chl *a*) concentrations (0.2-
38 0.6 µg L⁻¹) and dominated by dense biomass of *Trichodesmium* as well as UCYN-B and diatom-
39 diazotroph associations (*Rhizosolenia* with *Richelia*-detected by microscopy and *het-1 nifH* copies).
40 Station LDC was located at an ultra-oligotrophic area of the South Pacific gyre with extremely low Chl
41 *a* concentration (~ 0.02 µg L⁻¹) with limited biomass of diazotrophs predominantly the unicellular
42 UCYN-B. Our measurements of biomass from LDA and LDB yielded high activities of caspase-like
43 and metacaspase proteases that are indicative of PCD in *Trichodesmium* and other phytoplankton.
44 Metacaspase activity, reported here for the first time from oceanic populations, was highest at the surface
45 of both LDA and LDB, where we also obtained high concentrations of transparent exopolymeric
46 particles (TEP). TEP was negatively correlated with dissolved inorganic phosphorus and positively
47 coupled to both the dissolved and particulate organic carbon pools. Our results reflect the increase in
48 TEP production under nutrient stress and its role as a source of sticky carbon facilitating aggregation
49 and rapid vertical sinking. Evidence for bloom decline was observed at both LDA and LDB. However,
50 the physiological status and rates of decline of the blooms differed between the stations, influencing the
51 amount of accumulated diazotrophic organic matter and mass flux observed in the traps during our
52 experimental time frame. At LDA sediment traps contained the greatest export of particulate matter and
53 significant numbers of both intact and decaying *Trichodesmium*, UCYN-B, and *het-1* compared to LDB
54 where the bloom decline began only 2 days prior to leaving the station and to LDC where no evidence
55 for bloom or bloom decline was seen. Substantiating previous findings from laboratory cultures linking
56 PCD to carbon export in *Trichodesmium*, our results from OUTPACE indicate that PCD may be induced
57 by nutrient limitation in high biomass blooms such as *Trichodesmium* or diatom-diazotroph associations.
58 Furthermore, PCD combined with high TEP production will tend to facilitate cellular aggregation and
59 bloom termination and will expedite vertical flux to depth.

60

61

62

63

64

65

66

67

68 1. Introduction

69 The efficiency of the biological pump, essential in the transfer and sequestration of carbon to the
70 deep ocean, depends on the balance between growth (production) and death. Moreover, the manner in
71 which marine organisms die may ultimately determine the flow of fixed organic matter within the
72 aquatic environment and whether organic matter is incorporated into higher trophic levels, recycled
73 within the microbial loop sustaining subsequent production, or sink out (and exported) to depth.

74 N₂ fixing (diazotrophic) prokaryotic organisms are important contributors to the biological pump
75 and their ability to fix atmospheric N₂ confers an inherent advantage in the nitrogen-limited surface
76 waters of many oceanic regions. The oligotrophic waters of the Western Tropical South Pacific
77 (WTSP) have been characterized with some of the highest recorded rates of N₂ fixation (151-700 μmol
78 N m⁻² d⁻¹) (Garcia et al., 2007; Bonnet et al., 2005), and can reach up to 1200 μmol N m⁻² d⁻¹ (Bonnet et
79 al., 2017b). Diazotrophic communities comprised of unicellular cyanobacteria lineages (UCYN-A, B
80 and C), diatom-diazotroph associations such as *Richelia* associated with *Rhizosolenia*, and diverse
81 heterotrophic bacteria such as alpha and γ- protobacteria are responsible for these rates of N₂ fixation.
82 The most conspicuous of all diazotrophs, and predominating in terms of biomass, is the filamentous
83 bloom-forming cyanobacteria *Trichodesmium* forming massive surface blooms that supply ~ 60-80 Tg
84 N yr⁻¹ of the 100-200 Tg N yr⁻¹ of the estimated marine N₂ fixation (Capone et al., 1997; Carpenter et
85 al., 2004; Westberry and Siegel, 2006) with a large fraction fixed in the WTSP (Dupouy et al.,
86 2000; Dupouy et al., 2011; Tenorio et al., in review) that may, based- on NanoSIMS cell-specific
87 measurements, contribute up to ~ 80 % of bulk N₂ fixation rates in the WTSP (Bonnet et al., 2017a).

88 How *Trichodesmium* blooms form and develop has been investigated intensely while little data is
89 found regarding the fate of blooms. *Trichodesmium* blooms often collapse within 3-5 days, with
90 mortality rates paralleling bloom development rates (Rodier and Le Borgne, 2008; Rodier and Le
91 Borgne, 2010; Bergman et al., 2012). Cell mortality can occur due to grazing (O'Neil, 1998), viral lysis
92 (Hewson et al., 2004; Ohki, 1999), and/or programmed cell death (PCD) an autocatalytic genetically
93 controlled death (Berman-Frank et al., 2004). PCD is induced in response to oxidative and nutrient
94 stress, as has been documented in both laboratory and natural populations of *Trichodesmium* (Berman-
95 Frank et al., 2004; Berman-Frank et al., 2007) and in other phytoplankton (Bidle, 2015). The cellular
96 and morphological features of PCD in *Trichodesmium*, include elevated gene expression and activity
97 of metacaspases and caspase like-proteins; hallmark protein families involved in PCD pathways in
98 other organisms whose functions in *Trichodesmium* are currently unknown. PCD in *Trichodesmium*
99 also displays increased production of transparent exopolymeric particles (TEP) and trichome
100 aggregation as well as buoyancy loss vis a reduction in gas vesicles. This causes rapid sinking rates
101 that can be significant when large biomass such as that in oceanic blooms crashes (Bar-Zeev et al.,
102 2013; Berman-Frank et al., 2004).

103 Simulating PCD in laboratory cultures of *Trichodesmium* in 2 m water columns (Bar-Zeev et al.,
104 2013) led to a collapse of the *Trichodesmium* biomass and to greatly enhanced sinking of large
105 aggregates reaching rates of up to $\sim 200 \text{ m d}^{-1}$ that efficiently exported particulate organic carbon
106 (POC) and particulate organic nitrogen (PON) to the bottom of the water column. Although the
107 sinking rates and degree of export from this model system could not be extrapolated to the ocean, this
108 study mechanistically linked autocatalytic PCD and bloom collapse to quantitative C and N export
109 fluxes, suggesting that PCD may have an impact on the biological pump efficiency in the oceans (Bar-
110 Zeev et al., 2013).

111 We further examined this issue in the open ocean and investigated the cellular processes mediating
112 *Trichodesmium* mortality in a large surface bloom from the New Caledonian lagoon (Spungin et al.,
113 2016). Nutrient stress induced a PCD mediated crash of the *Trichodesmium* bloom. The filaments and
114 colonies were characterized by upregulated expression of metacaspase genes, downregulated
115 expression of gas-vesicle genes, enhanced TEP production, and aggregation of the biomass (Spungin
116 et al., 2016). Due to experimental conditions we could not measure the subsequent export and vertical
117 flux of the dying biomass in the open ocean. Moreover, while the existence and role of PCD and its
118 mediation of biogeochemical cycling of organic matter has been investigated in *Trichodesmium*,
119 scarce information exists about PCD and other mortality pathways of most marine diazotrophs.

120 The OUTPACE (Oligotrophy to UITra-oligotrophy PACific Experiment) cruise was conducted
121 from 18 February to 3 April 2015 along a west to east gradient from the oligotrophic area north of
122 New Caledonia to the ultraoligotrophic western South Pacific gyre (French Polynesia). The goal of the
123 OUTPACE experiment was to study the diazotrophic blooms and their fate within the oligotrophic
124 ocean in the Western Tropical South Pacific Ocean (Moutin et al., 2017). Our specific objective was to
125 determine whether PCD was an important mechanism affecting diazotroph mortality and a factor
126 regulating the fate of the blooms by mediation of vertical flux of organic matter. The strategy and
127 experimental approach of the OUTPACE transect enabled sampling at three long duration (LD)
128 stations of 5 days each (referred to as stations LDA, LDB, and LDC) and provided 5-day snapshots
129 into diazotroph physiology, dynamics, and mortality processes. We specifically probed for the
130 induction and operation of PCD and examined the relationship of PCD to the fate of organic matter
131 and vertical flux from diazotrophs by the deployment of 3 sediment traps at 150, 325 and 500 m
132 depths.

133

134

135

136

137 **2. Methods**

138

139 **2.1. Sampling site and sampling conditions**

140 Sampling was conducted on a transect during austral summer (18 Feb-5 Apr, 2015), on board the
141 R/V L'Atalante (Moutin et al., 2017). Samples were collected from three long duration stations (LD-
142 A, LD-B and LD-C) where the ship remained for 5 days at each location and 15 short duration (SD1-
143 15) stations (approximately eight hours duration). The cruise transect was divided into two geographic
144 regions. The first region (Melanesian archipelago, MA) included SD1-12, LDA and LDB stations
145 (160° E-178° E and 170°-175° W). The second region (subtropical gyre, GY) included SD 13-15 and
146 LDC stations (160° W-169° W).

147

148 **2.2. Chlorophyll *a***

149 Samples for determination of (Chl *a*) concentrations were collected by filtering 550 ml sea water
150 on GF/F filters (Whatman, UK). Filters were frozen and stored in liquid nitrogen, Chl *a* was extracted
151 in methanol and measured fluorometrically (Turner Designs Trilogy Optical kit) (Le Bouteiller et al.,
152 1992). Satellite derived surface Chl *a* concentrations at the LD stations were used from before and
153 after the cruise sampling at the LD stations. Satellite Chl *a* data are added as supplementary video files
154 (Supplementary videos S1, S2, S3).

155

156 **2.3. Caspase and metacaspase activities**

157 Biomass was collected on 25 mm, 0.2 µm pore-size polycarbonate filters and resuspended in 0.6-1
158 ml Lauber buffer [50 mM HEPES (pH 7.3), 100 mM NaCl, 10 % sucrose, 0.1 % (3-cholamidopropyl)-
159 dimethylammonio-1-propanesulfonate, and 10 mM dithiothreitol] and sonicated on ice (four cycles of
160 30 seconds each) using an ultracell disruptor (Sonic Dismembrator, Fisher Scientific, Waltham, MA,
161 USA). Cell extracts were centrifuged (10,000 x g, 2 min, room temperature), and the supernatant was
162 collected for caspase and metacaspase activity measurements. Caspase specific activity (normalized to
163 total protein concentration) was determined by measuring the kinetics of cleavage for the fluorogenic
164 caspase substrate Z-IETD-AFC (Z-Ile-Glu-Thr-Asp-AFC) at a 50 mM final concentration (using Ex
165 400 nm, Em 505 nm; Synergy4 BioTek, Winooski, VT, USA), as previously described in Bar-Zeev et
166 al. (2013). Metacaspase specific activity (normalized to total protein concentration) was determined by
167 measuring the kinetics of cleavage for the fluorogenic metacaspase substrate Ac-VRPR-AMC (Ac-
168 Val-Arg-Pro-Arg-AMC), (Klemenčič et al., 2015; Tsiatsiani et al., 2011) at a 50 mM final
169 concentration (using Ex 380 nm, Em 460 nm; Synergy4 BioTek, Winooski, VT, USA) (Klemenčič et
170 al., 2015; Tsiatsiani et al., 2011). Relative fluorescence units were converted to protein-normalized
171 substrate cleavage rates using AFC and AMC standards (Sigma) for caspase and metacaspase
172 activities, respectively. Total protein concentrations were determined by Pierce™ BCA protein assay
173 kit (Thermo Scientific product #23225).

174 **2.4. Phosphate analysis**

175 Seawater for phosphate (PO_4^{3-} , DIP) analysis was collected in 20 mL high-density polyethylene
176 HCL-rinsed bottles and poisoned with HgCl_2 to a final concentration of $20 \mu\text{g L}^{-1}$, stored at 4°C until
177 analysis. PO_4^{3-} was determined by a standard colorimetric technique using a segmented flow analyzer
178 according to Aminot and K  rouel (2007) on a SEAL Analytical AA3 HR system 20 (SEAL Analytica,
179 Serblabo Technologies, Entraigues Sur La Sorgue, France). Quantification limit for PO_4^{3-} was 0.05
180 $\mu\text{mol L}^{-1}$.

181

182 **2.5. Particulate organic carbon (POC) and nitrogen (PON)**

183 Samples were filtered through pre-combusted (4 h, 450°C) GF/F filters (Whatman GF/F, 25 mm),
184 dried overnight at 60°C and stored in a desiccator until further analysis. POC and PON were
185 determined using a CHN analyzer Perkin Elmer (Waltham, MA, USA) 2400 Series II CHNS/O
186 Elemental Analyzer after carbonate removal from the filters using overnight fuming with concentrated
187 HCl vapor.

188

189 **2.6. Dissolved organic carbon (DOC) and Total organic carbon (TOC)**

190 Samples were collected from the Niskin bottles in combusted glass bottles and were immediately
191 filtered through 2 precombusted (24 h, 450°C) glass fiber filters (Whatman GF/F, 25 mm). Filtered
192 samples were collected into glass precombusted ampoules that were sealed immediately after
193 filtration. Samples were acidified with orthophosphoric acid (H_3PO_4) and analyzed by high
194 temperature catalytic oxidation (HTCO) (Sugimura and Suzuki, 1988;Cauwet, 1994) on a Shimadzu
195 TOC-L analyzer. TOC was determined as POC+DOC.

196

197 **2.7. Transparent exopolymeric particles (TEP)**

198 Water samples (100 mL) were gently (< 150 mbar) filtered through a $0.45 \mu\text{m}$ polycarbonate filter
199 (GE Water & Process Technologies). Filters were then stained with a solution of 0.02 % Alcian Blue
200 (AB) and 0.06 % acetic acid (pH of 2.5), and the excess dye was removed by a quick deionized water
201 rinse. Filters were then immersed in sulfuric acid (80 %) for 2 h, and the absorbance (787 nm) was
202 measured spectrophotometrically (CARY 100, Varian). AB was calibrated using a purified
203 polysaccharide gum xanthan (GX) (Passow and Alldredge, 1995). TEP concentrations ($\mu\text{g GX}$
204 equivalents L^{-1}) were measured according to Passow and Alldredge (1995). To estimate the role of
205 TEP in C cycling, the total amount of TEP-C was calculated using the TEP concentrations at each
206 depth, and the conversion of GX equivalents to carbon applying the revised factor of 0.63 based on
207 empirical experiments from both natural samples from different oceanic areas and phytoplankton
208 cultures (Engel, 2004).

209 **2.8. Diazotrophic abundance**

210 The full description of DNA extraction, primer design and qPCR analyses are described in detail in
211 this issue (Stenegren et al., 2017). Briefly, 2.5 L of water from 6-7 depths with surface irradiance light
212 intensity (100, 75, 54, 36, 10, 1, and 0.1 %) were sampled and filtered onto a 25 mm diameter Supor
213 filter (Pall Corporation, PallNorden, AB Lund Sweden) with a pore size 0.2 µm filters. Filters were
214 stored frozen in pre-sterilized bead beater tubes (Biospec Bartlesville Ok, USA) containing 30 mL of
215 0.1 mm and 0.5 mm glass bead mixture. DNA was extracted from the filters using a modified protocol
216 of the Qiagen DNAeasy plant kit (Moisander et al., 2008) and eluted in 70 µL. With the re-eluted DNA
217 extracts ready, samples were analyzed using the qPCR instrument StepOnePlus (Applied Biosystems)
218 and fast mode. Previously designed TaqMAN assays and oligonucleotides and standards were prepared
219 in advance and followed previously described methods for the following cyanobacterial diazotrophs:
220 *Trichodesmium*, UCYN-A1, UCYN-A2, UCYN-B, *Richelia* symbionts of diatoms (het-1, het-2, het-3)
221 (Stenegren et al., 2017; Church et al., 2005; Foster et al., 2007; Moisander et al., 2010; Thompson et al.,
222 2012).

223 **2.9. Microscopy**

224 Samples for microscopy were collected in parallel from the same depth profiles for nucleic acid as
225 described in Stenegren et al. (2017). Briefly, 2 profiles were collected on day 1 and 3 at each LD station
226 and immediately filtered onto a 47 mm diameter Poretics (Millipore, Merck Millipore, Solna,
227 Sweden) membrane filter with a pore size of 5 µm using a peristaltic pump. After filtration samples
228 were fixed with a 1 % paraformaldehyde (v/v) for 30 min. prior to storing at -20 °C. The filters were
229 later mounted onto an oversized slide, and examined under an Olympus BX60 microscope equipped
230 with blue (460-490 nm) and green (545-580 nm) excitation wavelengths. Three areas (0.94 mm²) per
231 filter were counted separately and values were averaged. When abundances were low, the entire filter
232 (area=1734 mm²) was observed and cells enumerated. Due to poor fluorescence, only *Trichodesmium*
233 colonies and free-filaments could be accurately enumerated by microscopy, and in addition the larger
234 cell diameter *Trichodesmium* (*Katagnemene pelagicum*) was counted separately as these were often
235 present (albeit at lower densities). Other cyanobacterial diazotrophs (e.g. *Crocospaera watsonii*-like
236 cells, the *Richelia* symbionts of diatoms were present but with poor fluorescence and could only be
237 qualitatively noted.

238 **2.10. Particulate matter from sediment traps**

239 Particulate matter export was quantified with three PPS5 sediment traps (1 m² surface collection,
240 Technicap, France) deployed for 5 days at 150, 325 and 500 m at each LD station. Particle export was
241 recovered in polyethylene flasks screwed on a rotary disk which allowed flasks to be changed
242 automatically every 24-h to obtain a daily material recovery. The flasks were previously filled with a

243 buffered solution of formaldehyde (final conc. 2 %) and were stored at 4 °C until analysis to prevent
244 degradation of the collected material. The flask corresponding to the fifth day of sampling on the
245 rotary disk was not filled with formaldehyde to collect ‘fresh particulate matter’ for further diazotroph
246 quantification. Exported particulate matter was weighed and analyzed on EA-IRMS (Integra2, Sercon
247 Ltd) to quantify exported PC and PN.

248 **2.11. Diazotroph abundance in the traps**

249 Triplicate aliquots of 2-4 mL from the flask dedicated for diazotroph quantification were filtered
250 onto 0.2 µm Supor filters, flash frozen in liquid nitrogen and stored at -80 °C until analysis. Nucleic
251 acids were extracted from the filters as described in Moisander et al. (2008) with a 30 second
252 reduction in the agitation step in a Fast Prep cell disruptor (Thermo, Model FP120; Qbiogene, Inc.
253 Cedex, France) and an elution volume of 70 µl. Diazotroph abundance for *Trichodesmium* spp.,
254 UCYN-B, UCYN-A1, het-1, and het-2 were quantified by qPCR analyses on the *nifH* gene using
255 previously described oligonucleotides and assays (Foster et al., 2007; Church et al., 2005). The qPCR
256 was conducted using a StepOnePlus system (Applied Biosystems, Life Technologies, Stockholm
257 Sweden) with the following parameters: 50 °C for 2 min, 95°C for 10 min, and 45 cycles of 95°C for
258 15s followed by 60°C for 1 min. Gene copy numbers were calculated from the mean cycle threshold
259 (Ct) value of three replicates and the standard curve for the appropriate primer and probe set. For each
260 primer and probe set, duplicate standard curves were made from 10-fold dilution series ranging from
261 10⁸ to 1 gene copies per reaction. The standard curves were made from linearized plasmids of the
262 target *nifH* or from synthesized gBlocks gene fragments (IDT technologies, Cralville, Iowa USA).
263 Regression analyses of the results (number of cycles=Ct) of the standard curves were analyzed in
264 Excel. 2 µl of 5 KDa filtered nuclease free water was used for the no template controls (NTCs). No
265 *nifH* copies were detected for any target in the NTC. In some samples only 1 or 2 of the 3 replicates
266 produced an amplification signal; these were noted as detectable but not quantifiable (dnq). A 4th
267 replicate was used to estimate the reaction efficiency for the *Trichodesmium* and UCYN-B targets as
268 previously described in (Short et al., 2004). Seven and two samples were below 95 % in reaction
269 efficiency for *Trichodesmium* and UCYN-B, respectively. The detection limit for the qPCR assays is
270 1-10 copies.

271 **2.12. Statistics**

272 A Spearman correlation coefficient test was applied to examine the strength of association
273 between two variables and the direction of the relationship.

274

275 3. Results and discussion

276 3.1. Diazotrophic characteristics and abundance in the LD stations

277 The sampling strategy of the transect was planned so that changes in abundance and fate of
278 diazotrophs could be followed in “long duration” (LD) stations where measurements were taken from
279 the same water mass (and location) over 5 days and drifting sediment traps were deployed (Moutin et
280 al., 2017). Although rates for the different parameters were obtained for 5 days, this period is still a
281 “snapshot” in time with the processes measured influenced by preceding events and also continuing
282 after the ship departed. Specifically, production of photosynthetic biomass (as determined from
283 satellite-derived Chl *a*) and development of surface phytoplankton blooms, including cyanobacterial
284 diazotrophs, displayed specific characteristics for each of the LD stations. We first examined the
285 satellite-derived surface Chl *a* concentrations by looking at changes around the LD stations before and
286 after our 5 day sampling at each station [daily surface Chl *a* (mg m^{-3})] (Supplementary videos S1, S2,
287 S3).

288 At LDA, satellite data confirmed high concentrations of Chl *a* indicative of intense surface blooms
289 ($\sim 0.55 \mu\text{g L}^{-1}$) between 8th of February 2015 to 19th of February 2015 which began to gradually
290 decline with over 60 % Chl *a* reduction until day 1 at the station (Supplementary video S1, Fig. 1a).
291 By the time we reached LDA on 25.02.15 (day 1) Chl *a* concentrations averaged $\sim 0.2 \mu\text{g L}^{-1}$ Chl *a* at
292 the surface (Fig. 1a) and remained steady for the next 5 days with Chl *a* values of $0.2 \mu\text{g L}^{-1}$ measured
293 on day 5 (Fig 1a). When looking for biomass at depth the DCM recorded at ~ 80 m depth was
294 characterized by Chl *a* concentrations increasing from 0.4 to $0.5 \mu\text{g L}^{-1}$ between day 3 and 5
295 respectively (Fig. 1d). While the Chl *a* values of the surface biomass decreased for approximately one
296 week prior to our sampling at station, the Chl *a* concentrations measured at depth increased during the
297 corresponding time.

298 In contrast to LDA, the satellite data from LDB confirmed the presence of a surface bloom/s for
299 over one month prior to our arrival at the station on 15th of March 2015 (day 1) (Supplementary video
300 S2, Fig. 1b). This bloom was characterized by high surface Chl *a* concentrations ($\sim 0.6 \mu\text{g L}^{-1}$,
301 Supplementary video S2) and on day 1 at the station surface Chl *a* was $0.6 \mu\text{g L}^{-1}$ (Fig. 1b). Surface
302 Chl *a* then decreased over the next days at the station with a 50 % reduction of Chl *a* concentration
303 from the sea surface (5m) on day 5 ($0.4 \mu\text{g L}^{-1}$), (Fig. 1e). Thus, it appears that our 5 sampling days at
304 LDB were tracking a surface bloom that had only begun to decline after day 3 and continued to
305 decrease ($\sim 0.1 \mu\text{g L}^{-1}$) also after we have left (Fig.1b). On day 1 of sampling, the DCM at LDB was
306 relatively shallow, at 40 m with Chl *a* values of $0.5 \mu\text{g L}^{-1}$. By day 5 the DCM had deepened to 80 m
307 (de Verneil et al., 2017).

308 LDC was located in a region of extreme oligotrophy within the Cook Islands territorial waters
309 (GY waters). This station was characterized historically (~ 4 weeks before arrival) by extremely low

310 Chl *a* concentrations at the surface ($\sim 0.02 \mu\text{g L}^{-1}$, Supplementary video S3) that were an order of
311 magnitude lower than average Chl *a* measured at LDA and LDB. These values remained low with no
312 significant variability for the 5 days at station or later (Fig. 1f) (Supplementary video S3, Fig. 1c).
313 Similar to the results from LDA, the DCM at LDC was found near the bottom of the photic layer at \sim
314 135 m, with Chl *a* concentrations about 10-fold higher than those measured at surface with $\sim 0.2 \mu\text{g}$
315 L^{-1} (Fig. 1f).

316 Chl *a* is an indirect proxy of photosynthetic biomass and we thus needed to ascertain who the
317 dominant players (specifically targeting diazotrophic populations) were at each of the LD stations.
318 Moreover, At LDA and LDB diazotrophic composition and abundance as determined by qPCR
319 analysis were quite similar. At LDA *Trichodesmium* was the most abundant diazotroph, ranging
320 between 6×10^4 - 1×10^6 *nifH* copies L^{-1} in the upper water column (0-70 m). UCYN-B (genetically
321 identical to *Crocospaera watsonii*) co-occurred with *Trichodesmium* between 35 and 70 m, and het1
322 specifically identifying the diatom-diazotroph association (DDA) between the diatom *Rhizosolenia*
323 and the heterocystous diazotroph *Richelia*, was observed only at the surface waters at 4 m. UCYN-B
324 and het-1 abundances were relatively lower than *Trichodesmium* abundances with 2×10^2 *nifH* copies
325 L^{-1} and 3×10^3 *nifH* copies L^{-1} respectively (Stenegren et al., 2017). Microscopic observations from
326 LDA indicated that near the surface *Rhizosolenia* populations were already showing signs of decay
327 since the silicified cell-wall frustules were broken and free filaments of *Richelia* were observed (Fig.
328 2e-f) (Stenegren et al., 2017). DDAs are significant N_2 fixers in the oligotrophic oceans. Although
329 their abundance in the WTSP is usually low, they are common and highly abundant in the New
330 Caledonian lagoon significantly impacting C sequestration and rapid sinking (Turk-Kubo et al., 2015).

331 At LDB, *Trichodesmium* was also the most abundant diazotroph with *nifH* copies L^{-1} ranging
332 between 1×10^4 - 5×10^5 within the top 60 m (Stenegren et al., 2017). Microscopical analyses confirmed
333 high abundance of free filaments of *Trichodesmium* at LDB, while colonies were rarely observed
334 (Stenegren et al., 2017). Observations of poor cell integrity were reported for most collected samples,
335 with filaments at various stages of degradation and colonies under possible stress (Fig. 2a-d). In
336 addition to *Trichodesmium*, UCYN-B was the second most abundant diazotroph ranging between
337 1×10^2 and 2×10^3 *nifH* copies L^{-1} . Other unicellular diazotrophs of the UCYN groups (UCYN-A1 and
338 UCYN-A2) were the least detected diazotrophs (Stenegren et al., 2017). Of the three heterocystous
339 cyanobacterial symbiont lineages (het-1, het-2, het-3), het-1 was the most dominant (1×10^1 - 4×10^3 *nifH*
340 copies L^{-1}), (Stenegren et al., 2017). Microscopic analyses from LDB demonstrated the co-occurrence
341 of degrading diatom cells, mainly belonging to *Rhizosolenia* (Stenegren et al., 2017) (Fig. 2e-f).

342 In contrast to LDA and LDB, at LDC, the highest *nifH* copy numbers (up to 6×10^5 *nifH* copies L^{-1} at
343 60 m depth were from the unicellular diazotrophs UCYN-B (Stenegren et al., 2017) *Trichodesmium*

344 was only detected at 60 m and with very low copy numbers of *nifH* ($\sim 7 \times 10^2$ *nifH* copies L⁻¹)
345 (Stenegren et al., 2017).

346 Corresponding to the physiological status of the bloom, higher N₂ fixation rates (45.0 nmol N L⁻¹
347 d⁻¹) were measured in the surface waters (5m) of LDB in comparison with those measured at LDA and
348 LDC (19.3 nmol N L⁻¹ d⁻¹ in LDA and below the detection limit at LDC at 5m), (Caffin et al., 2017).

349 350 **3.2. Diazotrophic bloom demise in the LD stations**

351 Of the 3 long duration stations we examined, LDA and LDB had a higher biomass of diazotrophs
352 during the 5 days of sampling (section 3.1). Our analyses examining bloom dynamics from the
353 satellite-derived Chl *a* concentrations indicate a declining trend in chlorophyll-based biomass during
354 the sampling time period. Yet, both LDA and LDB were still characterized by high (and visible to the
355 eye at surface) biomass on the first sampling day at each station (day 1) as determined by qPCR and
356 microscopy (Stenegren et al., 2017). This is different from LDC where biomass was extremely limited,
357 and no clear evidence was obtained for any specific bloom or bloom demise. We therefore show
358 results mostly from LDA and LDB and focus specifically on the evidence for PCD and diazotroph
359 decline in areas with high biomass and surface blooms.

360 The mortality of phytoplankton at sea can be difficult to discern as it most probably results
361 from co-occurring processes including physical forces, chemical stressors, grazing, viral lysis, and/or
362 PCD. Here, we specifically focused on evidence for PCD and whether the influence of zooplankton
363 grazing on the diazotrophs and especially on *Trichodesmium* at LDA and LDB impacted bloom
364 dynamics. At LDA and LDB total zooplankton population was generally low. Total zooplankton
365 population at LDA ranged between 911-1900 individuals m⁻³ and in LDB between 1209-2188
366 individuals m⁻³ on day 1 and day 5 respectively. *Trichodesmium* is toxic and inedible to most
367 zooplankton excluding three species of harpacticoid zooplankton- *Macrosetella gracilis*, *Miracia*
368 *efferrata* and *Oculosetella gracilis* (O'Neil and Roman, 1994). During our sampling days at these
369 stations, *Macrosetella gracilis* a specific grazer of *Trichodesmium* comprised less than 1 % of the
370 total zooplankton community with another grazer *Miracia efferrata* comprising less than 0.1 % of total
371 zooplankton community. *Oculosetella gracilis* was not found at these stations. The low number of
372 harpacticoid zooplankton specifically grazing on *Trichodesmium* found in the LDA and LDB station,
373 refutes the possibility that grazing caused the massive demise of the bloom. Moreover, the toxicity of
374 *Trichodesmium* to many grazers (Rodier and Le Borgne, 2008; Kerbrat et al., 2011) could critically
375 limit the amount of *Trichodesmium*-derived recycled matter within the upper mixed layer.

376 Viruses have been increasingly invoked as key agents terminating phytoplankton blooms.
377 Phages may infect *Trichodesmium* (Brown et al., 2013; Hewson et al., 2004; Ohki, 1999) yet they
378 have not been demonstrated to terminate large surface blooms. Virus like particles were previously
379 enumerated from *Trichodesmium* samples during bloom demise, yet the numbers of virus-like

380 particles did not indicate that a massive, phage-induced lytic event of *Trichodesmium* occurred there
381 (Spungin et al., 2016). Virus infection may cause for the induction of PCD by causing an increased
382 production of reactive oxygen species (Vardi et al., 2012) which stimulates PCD in algal cells
383 (Berman-Frank et al., 2004; Bidle, 2015; Thamatrakoln et al., 2012). Viral attack can also directly
384 trigger PCD as part of an antiviral defense system (Bidle, 2015). Virus abundance and activity were
385 not enumerated in this study, so we cannot estimate their specific influence on mortality.

386 Limited availability of Fe and P induce PCD in *Trichodesmium* (Berman-Frank et al. 2004;
387 Bar-Zeev et al. 2013). At LDA and LDB, Fe concentrations at the time of sampling were relatively
388 high (> 0.5 nM), possibly due to island effects (de Verneil et al., 2017). Phosphorus availability, or
389 lack of phosphorus, can also induce PCD (Berman-Frank et al., 2004; Spungin et al., 2016). PO_4^{3-}
390 concentrations at the surface (0-40m) of LDA and LDB stations were extremely low around $0.05 \mu\text{mol}$
391 L^{-1} (de Verneil et al., 2017), possibly consumed by the high biomass and high growth rates of the
392 bloom causing nutrient stress and bloom mortality. PO_4^{3-} concentrations observed at LDC were above
393 the quantification limit with average values of $0.2 \mu\text{mol L}^{-1}$ in the 0-150 m depths (data not shown).
394 These limited P concentrations may curtail the extent of growth, induce PCD, and pose an upper limit
395 on biomass accumulation.

396 Here we compared, for the first time in oceanic populations, two PCD indices, caspase-like
397 and metacaspase activities, to examine the presence/operation of PCD in the predominant
398 phytoplankton (and diazotroph) populations along the transect. This was determined by the cleavage
399 of Z-IETD-AFC and Ac-VRPR-AFC substrates for caspase-like and metacaspase activities
400 respectively. We specifically show the results from LDA and LDB where biomass and activities were
401 detectable.

402 Classic caspases are absent in phytoplankton, including in cyanobacteria, and are unique to
403 metazoans and several viruses (Minina et al., 2017). In diverse phytoplankton the presence of a
404 caspase domain suffices to demonstrate caspase-like proteolytic activity that occurs upon PCD
405 induction when the caspase specific substrate Z-IETD-AFC is added (Berman-Frank et al., 2004; Bidle
406 and Bender, 2008; Bar-Zeev et al., 2013). Cyanobacteria and many diazotrophs contain genes that are
407 similar to caspases, the metacaspases-cysteine proteases. These proteases share structural properties
408 with caspases, specifically a histidine-cysteine catalytic dyad in the predicted active site (Tsiatsiani et
409 al., 2011). While the specific role and function/s of metacaspases genes are unknown, and cannot be
410 directly linked to gene expression, preliminary investigations have indicated that when PCD is induced
411 some of these genes are upregulated (Bidle and Bender, 2008; Spungin et al., 2016).

412 Of the abundant diazotrophic populations at LDA and LDB 12 metacaspases have previously
413 been identified in *Trichodesmium* spp. (Asplund-Samuelsson et al., 2012; Asplund-Samuelsson,
414 2015; Jiang et al., 2010; Spungin et al., 2016). Phylogenetic analysis of a wide diversity of truncated

415 metacaspase proteins, containing the conserved and characteristic caspase super family (CASC;
416 cl00042) domain structure, revealed metacaspase genes in both *Richelia intracellularis* (het-1) from
417 the diatom-diazotroph association and *Crocospaera watsonii* (a cultivated unicellular
418 cyanobacterium) which is genetically identical to the UCYN-B *nifH* sequences (Spungin et al.,
419 unpublished data).

420 We compared between metacaspase and caspase-like activities for the > 0.2 μm fraction
421 sampled assuming that the greatest activity would be due to the principle organisms contributing to the
422 biomass – i.e the diazotrophic cyanobacteria. Caspase-like activity and metacaspase activity were
423 specifically measured at all LD stations (days 1,3,5) at 5 depths between 0-200 m. Caspase-like
424 activity at the surface waters (50 m) at LDA, as determined by the cleavage of IETD-AFC substrate,
425 was between 2.3 to 2.8 ± 0.1 pM hydrolyzed mg protein⁻¹ min⁻¹ on days 1 and 3 respectively (Fig. 3a).
426 The highest activity was measured on day 5 at 50 m with 5.1 ± 0.1 pM hydrolyzed mg protein⁻¹ min⁻¹.
427 Similar trends were obtained at LDA for metacaspase activity as measured by the cleavage of the
428 VRPR-AMC substrate, containing an Arg residue at the P1 position, specific for metacaspase
429 cleavage, (Tsiatsiani et al., 2011; Klemenčič et al., 2015). High and similar metacaspase activities were
430 measured on days 1 and 3 (50 m) with 32 ± 4 and 35 ± 0.2 pM hydrolyzed mg protein⁻¹ min⁻¹
431 respectively (Fig. 3a). The highest metacaspase activity was measured on day 5 at 50 m with 59 ± 1 pM
432 hydrolyzed mg protein⁻¹ min⁻¹ with declining activity at greater depths (Fig. 3b).

433 Caspase-like activity at LDB, was similar for all sampling days, with the highest activity
434 recorded from the surface samples (ranging from 3 ± 0.1 to 4.5 ± 0.2 pM hydrolyzed mg protein⁻¹ min⁻¹
435 at 7 m depth and then decreasing with depth) (Fig. 3d). At day 3 caspase-like activity at LDB
436 increased at the surface with 4.5 ± 0.2 pM hydrolyzed mg protein⁻¹ min⁻¹ and then declined slightly by
437 day 5 back to 3 ± 0.1 pM hydrolyzed mg protein⁻¹ min⁻¹. The decrease in activity at the surface between
438 day 3 and 5 was accompanied by an increase in caspase-like activity measured in the DCM between
439 day 3 and 5 (Fig. 3d). Caspase-like activity at the DCM at day 3 (35 m) was 1 ± 0.4 pM hydrolyzed mg
440 protein⁻¹ min⁻¹ and by day 5 increased to 3 ± 0.1 pM hydrolyzed mg protein⁻¹ min⁻¹ for samples from 70
441 m depth. Thus, at LDB, caspase-like activity increased from day 1 to 5 and with depth, with higher
442 activities that initially were recorded at surface and then at depth coupled with the decline of the
443 bloom (Fig. 3d). Similar trends were obtained at LDB for metacaspase activity with 11.1 ± 0.9 pM
444 hydrolyzed mg protein⁻¹ min⁻¹ at the surface (7 m) on day 1. A 4-fold increase in activity was
445 measured at the surface on day 3 with 40.1 ± 5 pM hydrolyzed mg protein⁻¹ min⁻¹ (Fig. 3e). Similar high
446 activities were measured also on day 5 (Fig. 3e). However, the increase in activity was also
447 pronounced at depth of ~ 70 m and not only at the surface. Metacaspase activity at day 5 was the
448 highest with 40.3 ± 0.5 and 44.6 ± 5 pM hydrolyzed mg protein⁻¹ min⁻¹ at 7 and 70 m respectively (Fig
449 3e). The relatively low metacaspase activity measured on day 1 appears to correspond with the

450 stressed physiological status of the biomass just prior to increased mortality rates. Metacaspase
451 activity increased corresponding with the pronounced decline in Chl *a* from day 1 to day 5 (Fig. 1b).

452 The measured metacaspase activities were typically 10-fold higher than caspase-like activity
453 rates (Fig 3). Yet, metacaspase and caspase-like activities are significantly and positively correlated at
454 LDA and LDB ($r=0.8$, $p<0.05$ and $r=0.8$ $p<0.001$ for LDA and LDB respectively) (Fig. 3c and 3f).
455 Both findings (i.e. higher metacaspase activity and tight correlation between metacaspase and
456 caspases) were demonstrated specifically in cultures and natural populations of *Trichodesmium*
457 undergoing PCD (Spungin et al., in review). As our experiments find a significant positive correlation
458 between both activities, we have done a series of inhibitor experiments to test whether metacaspase are
459 substrate specific and are not the caspase-like activity we have examined (Spungin et al., in review). In
460 vitro treatment with antipain efficiently inhibited metacaspase activity, confirming the arginine-based
461 specificity of *Trichodesmium*. Our biochemical activity and inhibitor observations demonstrate that
462 metacaspases and caspases-like activities are likely distinct and are independently activated under
463 stress and coupled to PCD in our experiments of both laboratory and field populations. However,
464 caspase-like activity was somewhat sensitive to the metacaspase inhibitor, antipain, showing a ~30-
465 40% drop in activity. This hints at some catalytic crossover between these two catalytic activities in
466 *Trichodesmium* that further should be studied. We do not know what protein is responsible for the
467 caspase-specific activities and what drivers regulate it. Yet, the tight correlation between both
468 activities specifically for *Trichodesmium*, and here at LDA and LDB suggest that both activities occur
469 in the cell when PCD is induced. To date, we are not aware of any previous studies examining
470 metacaspase or caspase-like activity (or the existence of PCD) in diatom-diazotroph associations such
471 as *Rhizosolenia - Richelia*.

472 3.3. TEP dynamics and carbon pools

473 Transparent exopolymeric particles link between the particulate and dissolved carbon fractions
474 and act to augment the coagulation of colloidal precursors from the dissolved organic matter and from
475 biotic debris and to increase vertical carbon flux (Passow, 2002; Verdugo and Santschi, 2010). TEP
476 production also increases upon PCD induction – specifically in large bloom forming organisms such
477 as *Trichodesmium* (Berman-Frank et al., 2007; Bar-Zeev et al., 2013).

478 At LDA, TEP concentrations at 50 m depth were highest at day 1 with measured concentrations
479 of 562 ± 7 $\mu\text{g GX L}^{-1}$ (Table. 1) that appear to correspond with the declining physiological status of the
480 cells that were sampled at that time (Fig. 2a-d). TEP concentrations during days 3 and 5 decreased to
481 less than 350 $\mu\text{g GX L}^{-1}$, and it is possible that most of the TEP had been formed and sank prior to our
482 measurements in the LDA station.

483 At LDB, TEP concentrations at day 1 and 3 were similar with ~ 400 $\mu\text{g GX L}^{-1}$ at the surface (7
484 m) while concentrations decreased about 2-fold with depth, averaging at 220 ± 56 and 253 ± 32 $\mu\text{g GX}$

485 L⁻¹ (35-200 m) for day 1 and 3 respectively (Fig. 4a, Table 2). A significant (> 150 %) increase in TEP
486 concentrations was observed on day 5 compared to previous days, with TEP values of 597±69 µg GX
487 L⁻¹ at the surface (7m) (Fig 4b, Table 2). Although TEP concentrations were elevated at surface, the
488 difference in averaged TEP concentrations observed at the deeper depths (35-200 m) between day 3
489 (157±28 µg GX L⁻¹) and day 5 (253±32 GX L⁻¹) indicated that TEP from the surface was either
490 breaking down or sinking to depth (Fig. 4a, Table 2). The TEP concentrations from this study
491 correspond with values and trends reported from other marine environments (Engel, 2004;Bar-Zeev et
492 al., 2009) and specifically with TEP concentrations measured from the New Caledonian lagoon
493 (Berman-Frank et al., 2016).

494 TEP is produced by many phytoplankton including cyanobacteria under conditions uncoupling
495 growth from photosynthesis (i.e. nutrient but not carbon limitation) (Berman-Frank and Dubinsky,
496 1999;Passow, 2002;Berman-Frank et al., 2007). Decreasing availability of dissolved nutrients such as
497 nitrate and phosphate has been significantly correlated with increase in TEP concentrations in both
498 cultured phytoplankton and natural marine systems (Bar-Zeev et al., 2013;Brussaard et al., 2005;Engel
499 et al., 2002;Urbani et al., 2005). TEP production in *Trichodesmium* is enhanced as a function of
500 nutrient stress (Berman-Frank et al., 2007).

501 In the New Caledonian coral lagoon TEP concentrations were significantly and negatively
502 correlated with ambient concentrations of dissolved inorganic phosphorus (DIP) (Berman-Frank et al.,
503 2016). Here, at LDB a significant negative correlation of TEP with DIP was also observed (Fig. 4b,
504 $p=0.005$), suggesting that lack of phosphorus set a limit to continued biomass increase and stimulated
505 TEP production in the nutrient-stressed cells. TEP production was also significantly positively
506 correlated with metacaspase activity at all days (Fig. 4c, $p=0.03$) further indicating that biomass
507 undergoing PCD produced more TEP. In the diatom *Rhizosolenia setigera* TEP concentrations
508 increased during the stationary- decline phase (Fukao et al., 2010) and could also affect buoyancy.
509 Coupling between PCD and elevated production of TEP and aggregation has been previously shown in
510 *Trichodesmium* cultures (Berman-Frank et al., 2007;Bar-Zeev et al., 2013). Here we cannot confirm a
511 mechanistic link between nutrient stress, PCD induction, and TEP production, but show significant
512 correlations between these parameters measured at LDA and LDB with the declining diazotroph
513 blooms (Fig. 4c) (Spungin et al., 2016).

514 Furthermore, TEP concentrations at LDB were significantly positively correlated with TOC,
515 POC, and DOC (Fig. 4d-f) confirming the integral part of TEP in the cycling of carbon at this station.
516 Assuming a carbon content of 63 % (w/w), (Engel, 2004) we estimate that TEP contributes to the
517 organic carbon pool in the order of ~ 80-400 µg C L⁻¹ (Table 1 and Table 2) with the percentage of
518 TEP-C from TOC ranging between 0.08- 42 % and 11-32 % at LDA and LDB respectively (Table 1
519 and 2, taking into account spatial and temporal differences). Thus, at LDB, surface TEP-C increased
520 from 22 % at day 3 to 32 % of the TOC content at day 5. Yet, for the same time period a 2-fold

521 increase of TEP was measured at 200 m (11 % to 21 %). These results reflect the bloom status at LDB.
522 During bloom development; organic C and N are incorporated to the cells and little biotic TEP
523 production occurs while stationary growth (as long as photosynthesis continues) stimulates TEP
524 production (Berman-Frank and Dubinsky, 1999). When mortality exceeds growth, the presence of
525 large amounts of sticky TEP provide “hot spots” or substrates for bacterial activity and facilitate
526 aggregation of particles and enhanced sinking rates of aggregates as previously observed for
527 *Trichodesmium* (Bar-Zeev et al., 2013).

528 **3.4. Linking PCD-induced bloom demise to particulate C and N export**

529 Measurements of elevated rates of metacaspase and caspase-like activities and changes in TEP
530 concentrations are not sufficient to link PCD and vertical export of organic matter as demonstrated for
531 laboratory cultures of *Trichodesmium* (Bar-Zeev et al., 2013). To see whether PCD-induced mortality
532 led to enhanced carbon flux at sea we now examined mass flux and specific evidence for diazotrophic
533 contributions from the drifting sediment traps (150, 325 and 500 m) at LDA and LDB stations.

534 Mass flux at LDA increased with time, with the maximal mass flux rates obtained from the 150 m
535 trap (123 dry weight (DW) m⁻² d⁻¹) on day 4. The highest mass flux was 40 and 27 DW m⁻² d⁻¹ from
536 the deeper sediment traps (325 and 500 m traps respectively). Particulate C (PC) and particulate
537 nitrogen (PN) showed similar trends as the mass flux. At LDA, PC varied between 3.2-30 mg sample⁻¹
538 and PN ranged from 0.3-3.2 mg sample⁻¹ in the 150 m trap. At LDB, PC varied from 1.6 to 6 mg
539 sample⁻¹ and total PN ranged from 0.2 to 0.8 mg sample⁻¹ in the 150 m trap. The total sediment flux in
540 the traps deployed at LDB ranged between 6.4 mg m⁻² d⁻¹ (150 m, day 4) and 33.5 mg m⁻² d⁻¹ (500 m,
541 day 2), with an average of 18.9 mg m⁻² d⁻¹. Excluding the deepest trap at 500 m where the high flux
542 occurred at day 2, in the other traps the highest export flux rate occurred at the last day at the station
543 (day 5).

544 Analyses of the community found in the sediment traps, determined by qPCR from the
545 accumulated matter on day 5 at the station, confirmed that *Trichodesmium*, UCYN-B and het-1 were
546 the most abundant diazotrophs in the sediment traps at LDA and LDB stations (Caffin et al., 2017),
547 significantly correlating with the dominant diazotrophs found at the surface of the ocean (measured on
548 day 1). *Trichodesmium* and *Rhizosolenia-Richelina* association (het-1) were the major contributors to
549 diazotroph export at LDA and LDB while UCYN-B and het-1 were the major contributors at LDC
550 (Caffin et al., 2017). At LDA the deeper traps contained *Trichodesmium* with 2.6 x10⁷ and 1.4x10⁷
551 *nifH* copies L⁻¹ at the 325 and 500 m traps respectively. UCYN-B was detected in all traps with the
552 highest abundance at the 325 m (4.2x10⁶ *nifH* copies L⁻¹) and 500 m traps (2.8x10⁶ *nifH* copies L⁻¹).
553 Het-1 was found only in the 325 m trap with 2.0x10⁷ *nifH* copies L⁻¹ (Fig. 5a). At LDB,
554 *Trichodesmium*, UCYN-B and het-1 were detected at the 325 and 500 m traps but not at 150 m.
555 *Trichodesmium* counts were 9x10⁵ at the 325 m trap and 5x10⁶ *nifH* copies L⁻¹ for the 500 m trap (Fig.

556 5b). While evidence for UCYN-B showed 3.6×10^5 and 10×10^5 *nifH* copies L⁻¹ at 325 and the 500 m
557 traps respectively (Fig. 5b).

558 In addition to exported *Trichodesmium* and *Rhizosolenia-Richelia* association, the small
559 unicellular UCYN-B (< 4 μ m) were also found in the sediment traps, including the deeper (500 m)
560 traps. UCYN-B is often associated with larger phytoplankton such as the diatom *Climacodium*
561 *frauenfeldianum* (Bench et al., 2013) or in colonial phenotypes (> 10 μ m fraction) as has been
562 observed in the northern tropical Pacific (ALOHA) (Foster et al., 2013). Sedimenting UCYN-B were
563 detected during the VAHINE mesocosm experiment in the New Caledonian lagoon in shallow (15m)
564 sediment traps) (Bonnet et al., 2015) and were also highly abundant in a floating sediment trap
565 deployed at 75 m for 24 h in the North Pacific Subtropical Gyre (Sohm et al., 2011). Thus our data
566 substantiates earlier conclusions that UCYN, which form large aggregates (increasing actual size and
567 sinking velocities), can efficiently contribute to export in oligotrophic systems (Bonnet et al., 2015).
568 Increase in aggregate size could also occur with depth, possibly due to the high concentrations of TEP
569 produced at the surface layer, sinking in the water column, providing a nutrient source and enhancing
570 aggregation (Berman-Frank et al., 2016).

571 The sinking rates of aggregates in the water column, depend on factors such as fluid viscosity,
572 particle source material, morphology, density, and variable particle characteristics. Sinking velocities
573 of diatoms embedded in aggregates are generally fast (50-200 m d⁻¹) (Asper, 1987; Alldredge, 1998)
574 compared with those of individually sinking cells (1⁻¹⁰ m d⁻¹) (Culver and Smith, 1989) allowing
575 aggregated particles to sink out of the photic zone to depth. Assuming a sinking rate of
576 *Trichodesmium*-based aggregates of 150-200 m d⁻¹ (Bar-Zeev et al., 2013), we would need to shift the
577 time frame by 1 day to see whether PCD measured from the surface waters is coupled with changes in
578 organic matter reflected in the 150 m sediment traps. Thus, at LDA, examining metacaspase activities
579 from the surface with mass flux and particulate matter obtained 24 h later yielded a significant positive
580 correlation between these two parameters (Fig. 5c).

581 LDA had the highest export flux and particulate matter found in its traps relative to LDB and
582 LDC. Diazotrophs contributed ~ 36 % to PC export in the 325 m trap at LDA, with *Trichodesmium*
583 comprising the bulk of diazotrophs (Caffin et al., 2017) In contrast, at LDB, we found lower flux rates
584 and lower organic material in the traps with *Trichodesmium* contributing the bulk of diazotroph
585 biomass at the 150 m trap. We believe that at LDB the decline phase began only halfway through our
586 sampling and thus the resulting export efficiency we obtained for the 5 days at station was relatively
587 low compared to the total amount of surface biomass. Moreover, considering export rates, and the
588 experimental time frame, most of the diazotrophic population may have been directly exported to the
589 traps only after we left the station (i.e. time frame > 5 days). This situation is different from the bloom
590 at LDA, where enhanced mortality, biomass deterioration, and bloom crash were initiated 1-2 weeks

591 before our arrival and sampling at the station. Thus, at LDA, elevated mass flux and higher
592 concentrations of organic matter were obtained from all three depths of the deployed traps.

593 In the field, especially in the surface layers of the oligotrophic oceanic regions, dead cells are rarely
594 seen at later stages (Berges and Choi 2014) or not seen (Segovia et al., 2018). This is due to the fact
595 that dying and dead cells are utilized quickly and recycled within the food web and upper surface layer.
596 However, under bloom conditions, when biomass is high, the fate of the extensive biomass is more
597 complicated (Bonnet et al., 2015). PCD induced cell death, combined with buoyancy loss, can lead to
598 rapid sinking to depth of the biomass at a speed that would prevent large feeding events on this biomass.
599 This may be determined by POC downward fluxes easy to measure in the lab and extremely complex
600 in the open ocean. We previously measured POC export in our lab under controlled conditions (Bar-
601 Zeev et al., 2013). Here, using sediment traps we have measured POC fluxes, but also have specific
602 indications (*NifH* reads) of *Trichodesmium* and other diazotrophs which were blooming for several days
603 at the surface. This indicates that under bloom conditions when biomass is high some of the cell pellets
604 do sink down out of the food web.

605

606 **4. Conclusion and implications**

607 Our specific objective in this study was to examine whether diazotroph mortality mediated by
608 PCD can lead to higher fluxes of organic matter sinking to depth. The OUTPACE cruise provided this
609 opportunity in two out of three long-duration (5 day) stations where large surface blooms of
610 diazotrophs principally comprised of *Trichodesmium*, UCYN-B and diatom-diazotroph associations
611 *Rhizosolenia-Richelina* and were encountered. We demonstrate (to our knowledge for the first time)
612 metabolically active metacaspases in oceanic populations of *Richelia* and *Trichodesmium*. Moreover,
613 metacaspase activities were significantly correlated to caspase-like activities at both LDA and LDB
614 stations with both protein families characteristic of PCD induced mortality. Evidence from drifting
615 sediment traps, deployed for 5 days at the two stations, showed high TEP concentrations formed at
616 surface and shifting to depth, increasing numbers of diazotrophs in sediment traps from 150, 350, 500
617 m depths), and a time-shifted correlation between metacaspase activity (signifying PCD) and vertical
618 flux of PC and PN).

619 Yet, our results also delineate the natural variability of biological oceanic populations. The two
620 stations, LDA and LDB were characterized by biomass at physiologically different stages. The
621 biomass from LDA displayed more pronounced mortality that had begun prior to our arrival at station.
622 In contrast, satellite data indicated that at LDB, the surface *Trichodesmium* bloom was sustained for at
623 least a month prior to the ship's arrival and remained high for the first 3 days of our sampling before
624 declining by 40 % at day 5. As sediment trap material was examined during a short time frame, of
625 only 5 days at each LD station, we assume that a proportion of the sinking diazotrophs and organic
626 matter were not yet collected in the traps and had either sunk before trap deployment or would sink

627 after we left the stations. Thus, these different historical conditions which influence physiological
628 status at each location also impacted the specific results we obtained and emphasized a-priori the
629 importance of comprehensive spatial and temporal sampling that would facilitate a more holistic
630 understanding of the dynamics and consequences of bloom formation and fate in the oceans.

631

632 **Author contributions**

633 IBF, DS, and SB conceived and designed the investigation linking PCD to vertical flux within the
634 OUTPACE project. NB, MS, AC, MPP, NL CD and RAF participated, collected and performed analyses
635 of samples, DS analysed samples and data. DS and IBF wrote the manuscript with contributions from
636 all co-authors.

637

638 **Acknowledgments**

639 This research is a contribution of the OUTPACE (Oligotrophy from Ultra-oligoTrophy PACific
640 Experiment) project (<https://outpace.mio.univ-amu.fr/>) funded by the Agence Nationale de la
641 Recherche (grant ANR-14-CE01-0007-01), the LEFE-CyBER program (CNRS-INSU), the Institut de
642 Recherche pour le Développement (IRD), the GOPS program (IRD) and the CNES (BC T23, ZBC
643 4500048836). The OUTPACE cruise (<http://dx.doi.org/10.17600/15000900>) was managed by the MIO
644 (OSU Institut Pytheas, AMU) from Marseilles (France). The authors thank the crew of the R/V
645 L'Atalante for outstanding shipboard operations. G. Rougier and M. Picheral are warmly thanked for
646 their efficient help in CTD rosette management and data processing, as well as C. Schmechtig for the
647 LEFE-CyBER database management. Aurelia Lozingot is acknowledged for the administrative work.
648 All data and metadata are available at the following web address: [http://www.obs-
649 vlfr.fr/proof/php/outpace/outpace.php](http://www.obs-
649 vlfr.fr/proof/php/outpace/outpace.php). We thank Olivier Grosso (MIO) and Sandra Hélias (MIO) for
650 the phosphate data and François Catlotti (MIO) for the zooplankton data. The ocean color satellite
651 products were provided by CLS in the framework of the CNES-OUTPACE project (PI A.M. Doglioli)
652 and the video is courtesy of A. de Verneil. RAF acknowledges Stina Höglund and the Image Facility
653 of Stockholm University and the Wenner-Gren Institute for access and assistance in confocal
654 microscopy. The participation of NB, DS, and IBF in the OUTPACE experiment was supported
655 through a collaborative grant to IBF and SB from Israel Ministry of Science and Technology Israel
656 and the High Council for Science and Technology (HCST)-France 2012/3-9246, and United States-
657 Israel Binational Science Foundation (BSF) grant No. 2008048 to IBF. RAF was funded by the Knut
658 and Alice Wallenberg Stiftelse, and acknowledges the helpful assistance of Dr. Lotta Berntzon. This
659 work is in partial fulfillment of the requirements for a PhD thesis for D. Spungin at Bar- Ilan
660 University.

661

662 **References**

- 663 Alldredge, A.: The carbon, nitrogen and mass content of marine snow as a function of aggregate size,
664 Deep Sea Research Part I: Oceanographic Research Papers, 45, 529-541, 1998.
- 665 Aminot, A., and K  rouel, R.: Dosage automatique des nutriments dans les eaux marines: m  thodes en
666 flux continu, Editions Quae, 2007.
- 667 Asper, V. L.: Measuring the flux and sinking speed of marine snow aggregates, Deep Sea Research
668 Part A. Oceanographic Research Papers, 34, 1-17, 1987.
- 669 Asplund-Samuelsson, J., Bergman, B., and Larsson, J.: Prokaryotic caspase homologs: phylogenetic
670 patterns and functional characteristics reveal considerable diversity, PLoS One, 7, e49888, 2012.
- 671 Asplund-Samuelsson, J.: The art of destruction: revealing the proteolytic capacity of bacterial caspase
672 homologs, Molecular microbiology, 98, 1-6, 2015.
- 673 Bar-Zeev, E., Berman-Frank, I., Liberman, B., Rahav, E., Passow, U., and Berman, T.: Transparent
674 exopolymer particles: Potential agents for organic fouling and biofilm formation in desalination and
675 water treatment plants, Desalination and Water Treatment, 3, 136-142, 2009.
- 676 Bar-Zeev, E., Avishay, I., Bidle, K. D., and Berman-Frank, I.: Programmed cell death in the marine
677 cyanobacterium *Trichodesmium* mediates carbon and nitrogen export, The ISME journal, 7, 2340-
678 2348, 2013.
- 679 Bench, S. R., Heller, P., Frank, I., Arciniega, M., Shilova, I. N., and Zehr, J. P.: Whole genome
680 comparison of six *Crocospaera watsonii* strains with differing phenotypes, Journal of phycology, 49,
681 786-801, 2013.
- 682 Bergman, B., Sandh, G., Lin, S., Larsson, J., and Carpenter, E. J.: *Trichodesmium* - a widespread
683 marine cyanobacterium with unusual nitrogen fixation properties, FEMS Microbiol Rev, 1-17, 2012.
- 684 Berman-Frank, I., and Dubinsky, Z.: Balanced growth in aquatic plants: Myth or reality?
685 Phytoplankton use the imbalance between carbon assimilation and biomass production to their
686 strategic advantage, Bioscience, 49, 29-37, 1999.
- 687 Berman-Frank, I., Bidle, K., Haramaty, L., and Falkowski, P.: The demise of the marine
688 cyanobacterium, *Trichodesmium* spp., via an autocatalyzed cell death pathway, Limnol. Oceanogr.,
689 49, 997-1005, 2004.
- 690 Berman-Frank, I., Rosenberg, G., Levitan, O., Haramaty, L., and Mari, X.: Coupling between
691 autocatalytic cell death and transparent exopolymeric particle production in the marine
692 cyanobacterium *Trichodesmium*, Environmental Microbiology, 9, 1415-1422, 10.1111/j.1462-
693 2920.2007.01257.x, 2007.
- 694 Berman-Frank, I., Spungin, D., Rahav, E., Wambeke, F. V., Turk-Kubo, K., and Moutin, T.:
695 Dynamics of transparent exopolymer particles (TEP) during the VAHINE mesocosm experiment in
696 the New Caledonian lagoon, Biogeosciences, 13, 3793-3805, 2016.
- 697 Bidle, K. D., and Bender, S. J.: Iron starvation and culture age activate metacaspases and programmed
698 cell death in the marine diatom *Thalassiosira pseudonana*, Eukaryotic Cell, 7, 223-236,
699 10.1128/ec.00296-07, 2008.
- 700 Bidle, K. D.: The molecular ecophysiology of programmed cell death in marine phytoplankton,
701 Annual review of marine science, 7, 341-375, 2015.

702 Bonnet, S., Guieu, U., Chiaverini, J., Ras, J., and Stock, A.: Effect of atmospheric nutrients on the
703 autotrophic communities in a low nutrient, low chlorophyll system, *Limnology and Oceanography*, 50,
704 1810-1819, 2005.

705 Bonnet, S., Berthelot, H., Turk-Kubo, K., Fawcett, S., Rahav, E., l'Helguen, S., and Berman-Frank, I.:
706 Dynamics of N₂ fixation and fate of diazotroph-derived nitrogen in a low nutrient low chlorophyll
707 ecosystem: results from the VAHINE mesocosm experiment (New Caledonia), *Biogeosciences*, 12,
708 19579-19626, doi:10.5194/bgd-12-19579-2015, 2015.

709 Bonnet, S., Caffin, M., Berthelot, H., Grosso, O., Guieu, C., and Moutin, T.: Contribution of dissolved
710 and particulate fractions to the Hot Spot of N₂ fixation in the Western Tropical South Pacific Ocean
711 (OUTPACE cruise), *Biogeosciences*, in review, 2017a.

712 Bonnet, S., Caffin, M., Berthelot, H., and Moutin, T.: Hot spot of N₂ fixation in the western tropical
713 South Pacific pleads for a spatial decoupling between N₂ fixation and denitrification, *Proceedings of*
714 *the National Academy of Sciences*, 114, E2800-E2801, 10.1073/pnas.1619514114, 2017b.

715 Brown, J. M., LaBarre, B. A., and Hewson, I.: Characterization of *Trichodesmium*-associated viral
716 communities in the eastern Gulf of Mexico, *FEMS Microbiol. Ecol.*, 84, 603–613, 2013

717 Brussaard, C. P. D., Mari, X., Van Bleijswijk, J. D. L., and Veldhuis, M. J. W.: A mesocosm study of
718 *Phaeocystis globosa* (Prymnesiophyceae) population dynamics - II. Significance for the microbial
719 community, *Harmful Algae*, 4, 875-893, 2005.

720 Caffin, M., Moutin, T., Foster, R. A., Bouruet-Aubertot, P., Doglioli, A. M., Berthelot, H., Grosso, O.,
721 Helias-Nunige, S., Leblond, N., and Gimenez, A.: Nitrogen budgets following a Lagrangian strategy
722 in the Western Tropical South Pacific Ocean: the prominent role of N₂ fixation (OUTPACE cruise),
723 *Biogeosciences* In review, 2017.

724 Capone, D. G., Zehr, J. P., Paerl, H. W., Bergman, B., and Carpenter, E. J.: *Trichodesmium*, a globally
725 significant marine cyanobacterium, *Science*, 276, 1221-1229, 1997.

726 Carpenter, E. J., Subramaniam, A., and Capone, D. G.: Biomass and primary productivity of the
727 cyanobacterium *Trichodesmium* spp. in the tropical N Atlantic ocean, *Deep-Sea Research Part I-*
728 *Oceanographic Research Papers*, 51, 173-203, 10.1016/j.dsr.2003.10.006, 2004.

729 Cauwet, G.: HTCO method for dissolved organic carbon analysis in seawater: influence of catalyst on
730 blank estimation, *Marine Chemistry*, 47, 55-64, 1994.

731 Choi CJ, Berges JA. New types of metacaspases in phytoplankton reveal diverse origins of cell death
732 proteases . *Cell Death and Disease*, 4, e490; doi:10.1038/cddis.2013.21, 2013.

733 Church, M. J., Jenkins, B. D., Karl, D. M., and Zehr, J. P.: Vertical distributions of nitrogen-fixing
734 phylotypes at Stn ALOHA in the oligotrophic North Pacific Ocean, *Aquatic Microbial Ecology*, 38, 3-
735 14, 2005.

736 Culver, M. E., and Smith, W. O.: Effects of environmental variation on sinking rates of marine
737 phytoplankton, *Journal of phycology*, 25, 262-270, 1989.

738 de Verneil, A., Rousselet, L., Doglioli, A. M., Petrenko, A. A., and Moutin, T.: The fate of a southwest
739 Pacific bloom: gauging the impact of submesoscale vs. mesoscale circulation on biological gradients
740 in the subtropics, *Biogeosciences*, 14, 3471, 2017.

- 741 Dupouy, C., Neveux, J., Subramaniam, A., Mulholland, M. R., Montoya, J. P., Campbell, L., Capone,
742 D. G., and Carpenter, E. J.: Satellite captures *Trichodesmium* blooms in the SouthWestern Tropical
743 Pacific., EOS, Trans American Geophysical Union., 81, 13-16, 2000.
- 744 Dupouy, C., Benielli-Gary, D., Neveux, J., Dandonneau, Y., and Westberry, T. K.: An algorithm for
745 detecting *Trichodesmium* surface blooms in the South Western Tropical Pacific, Biogeosciences, 8,
746 3631-3647, 10.5194/bg-8-3631-2011, 2011.
- 747 Engel, A., Goldthwait, S., Passow, U., and Alldredge, A.: Temporal decoupling of carbon and nitrogen
748 dynamics in a mesocosm diatom bloom, Limnology and Oceanography, 47, 3, 753-761, 2002.
- 749 Engel, A.: Distribution of transparent exopolymer particles (TEP) in the northeast Atlantic Ocean and
750 their potential significance for aggregation processes, Deep-Sea Research Part I-Oceanographic
751 Research Papers, 51, 83-92, 2004.
- 752 Foster, R. A., Subramaniam, A., Mahaffey, C., Carpenter, E. J., Capone, D. G., and Zehr, J. P.:
753 Influence of the Amazon River plume on distributions of free-living and symbiotic cyanobacteria in
754 the western tropical north Atlantic Ocean, Limnology and Oceanography, 52, 517-532, 2007.
- 755 Foster, R. A., Szejtjenzus, S., and Kuypers, M. M.: Measuring carbon and N₂ fixation in field
756 populations of colonial and free-living unicellular cyanobacteria using nanometer-scale secondary ion
757 mass spectrometry, Journal of phycology, 49, 502-516, 2013.
- 758 Fukao, T., Kimoto, K., and Kotani, Y.: Production of transparent exopolymer particles by four diatom
759 species, Fisheries science, 76, 755-760, 2010.
- 760 Garcia, N., Raimbault, P., and Sandroni, V.: Seasonal nitrogen fixation and primary production in the
761 Southwest Pacific: nanoplankton diazotrophy and transfer of nitrogen to picoplankton organisms,
762 Marine Ecology Progress Series, 343, 25-33, 2007.
- 763 Hewson, I., Govil, S. R., Capone, D. G., Carpenter, E. J., and Fuhrman, J. A.: Evidence of
764 *Trichodesmium* viral lysis and potential significance for biogeochemical cycling in the oligotrophic
765 ocean, Aquatic Microbial Ecology, 36, 1-8, 2004.
- 766 Jiang, X. D., Lonsdale, D. J., and Gobler, C. J.: Grazers and vitamins shape chain formation in a
767 bloom-forming dinoflagellate, *Cochlodinium polykrikoides*, Oecologia, 164, 455-464,
768 10.1007/s00442-010-1695-0, 2010.
- 769 Kerbrat, A. S., Amzil, Z., Pawlowicz, R., Golubic, S., Sibat, M., Darius, H. T., Chinain, M., and
770 Laurent, D.: First evidence of palytoxin and 42-hydroxy-palytoxin in the marine cyanobacterium
771 *Trichodesmium*, Marine drugs, 9, 543-560, 2011.
- 772 Klemenčič, M., Novinec, M., and Dolinar, M.: Orthocaspases are proteolytically active prokaryotic
773 caspase homologues: the case of *Microcystis aeruginosa*, Molecular microbiology, 98, 142-150, 2015.
- 774 Le Bouteiller, A., Blanchot, J., and Rodier, M.: Size distribution patterns of phytoplankton in the
775 western Pacific: towards a generalization for the tropical open ocean, Deep Sea Research Part A.
776 Oceanographic Research Papers, 39, 805-823, 1992.
- 777 Minina, E., Coll, N., Tuominen, H., and Bozhkov, P.: Metacaspases versus caspases in development
778 and cell fate regulation, Cell Death and Differentiation, 24, 1314, 2017.
- 779 Moisander, P. H., Beinart, R. A., Voss, M., and Zehr, J. P.: Diversity and abundance of diazotrophic
780 microorganisms in the South China Sea during intermonsoon, Isme Journal, 2, 954-967,
781 10.1038/ismej.2008.51, 2008.

- 782 Moisaner, P. H., Beinart, R. A., Hewson, I., White, A. E., Johnson, K. S., Carlson, C. A., Montoya, J.
783 P., and Zehr, J. P.: Unicellular Cyanobacterial Distributions Broaden the Oceanic N-2 Fixation
784 Domain, *Science*, 327, 1512-1514, 10.1126/science.1185468, 2010.
- 785 Moutin, T., Doglioli, A. M., De Verneil, A., and Bonnet, S.: Preface: The Oligotrophy to the UITra-
786 oligotrophy PACific Experiment (OUTPACE cruise, 18 February to 3 April 2015), *Biogeosciences*,
787 14, 3207, 2017.
- 788 O'Neil, J. M., and Roman, M. R.: Ingestion of the Cyanobacterium *Trichodesmium* spp by Pelagic
789 Harpacticoid Copepods *Macrosetella*, *Miracia* and *Oculostella*, *Hydrobiologia*, 293, 235-240, 1994.
- 790 O'Neil, J. M.: The colonial cyanobacterium *Trichodesmium* as a physical and nutritional substrate for
791 the harpacticoid copepod *Macrosetella gracilis*, *Journal of Plankton Research*, 20, 43-59, 1998.
- 792 Ohki, K.: A possible role of temperate phage in the regulation of *Trichodesmium* biomass, *Bulletin de*
793 *l'institute oceanographique*, Monaco, 19, 287-291, 1999.
- 794 Passow, U., and Alldredge, A. L.: A dye binding assay for the spectrophotometric measurement of
795 transparent exopolymer particles (TEP), *Limnol. & Oceanogr*, 40, 1326-1335, 1995.
- 796 Passow, U.: Transparent exopolymer particles (TEP) in aquatic environments, *Progress in*
797 *Oceanography*, 55, 287-333, 2002.
- 798 Rodier, M., and Le Borgne, R.: Population dynamics and environmental conditions affecting
799 *Trichodesmium* spp. (filamentous cyanobacteria) blooms in the south-west lagoon of New Caledonia,
800 *Journal of Experimental Marine Biology and Ecology*, 358, 20-32, 10.1016/j.jembe.2008.01.016,
801 2008.
- 802 Rodier, M., and Le Borgne, R.: Population and trophic dynamics of *Trichodesmium thiebautii* in the
803 SE lagoon of New Caledonia. Comparison with *T. erythraeum* in the SW lagoon, *Marine Pollution*
804 *Bulletin*, 61(7-12), 349-359, 10.1016/j.marpolbul.2010.06.018, 2010.
- 805 Segovia, M., Lorenzo, M.R., Iñiguez, C., García-Gómez C.: Physiological stress response associated
806 with elevated CO₂ and dissolved iron in a phytoplankton community dominated by the
807 coccolithophore *Emiliana huxleyi*. *Mar. Ecol. Prog. Ser.* 586-73-89, 2018.
- 808 Short, S. M., Jenkins, B. D., and Zehr, J. P.: Spatial and temporal distribution of two diazotrophic
809 bacteria in the Chesapeake Bay, *Applied and Environmental Microbiology*, 70, 2186-2192, 2004.
- 810 Sohm, J. A., Edwards, B. R., Wilson, B. G., and Webb, E. A.: Constitutive extracellular
811 polysaccharide (EPS) production by specific isolates of *Crocospaera watsonii*, *Frontiers in*
812 *microbiology*, 2, 2011.
- 813 Spungin, D., Pfreundt, U., Berthelot, H., Bonnet, S., AlRoumi, D., Natale, F., Hess, W. R., Bidle, K.
814 D., and Berman-Frank, I.: Mechanisms of *Trichodesmium* demise within the New Caledonian lagoon
815 during the VAHINE mesocosm experiment, *Biogeosciences*, 13, 4187-4203, 2016.
- 816 Stenegren, M., Caputo, A., Berg, C., Bonnet, S., and Foster, R. A.: Distribution and drivers of
817 symbiotic and free-living diazotrophic cyanobacteria in the Western Tropical South Pacific, *Biosci.*
818 *Discuss*, 1-47, 2017.
- 819 Sugimura, Y., and Suzuki, Y.: A high-temperature catalytic oxidation method for the determination of
820 non-volatile dissolved organic carbon in seawater by direct injection of a liquid sample, *Marine*
821 *Chemistry*, 24, 105-131, 1988.

822 Tenorio, M., Dupouy C., Rodier, M., and Neveux, J.: *Trichodesmium* and other Filamentous
823 Cyanobacteria in New Caledonian waters (South West Tropical Pacific) during an El Niño Episode,
824 *Aquatic Microbial Ecology*, in review.

825 Thamatrakoln, K., Korenovska, O., Niheu, A. K., and Bidle, K. D.: Whole-genome expression
826 analysis reveals a role for death-related genes in stress acclimation of the diatom *Thalassiosira*
827 *pseudonana*, *Environ. Microbiol.*, 14, 67–81, 2012.

828 Thompson, A. W., Foster, R. A., Krupke, A., Carter, B. J., Musat, N., Vaultot, D., Kuypers, M. M., and
829 Zehr, J. P.: Unicellular cyanobacterium symbiotic with a single-celled eukaryotic alga, *Science*, 337,
830 1546-1550, 2012.

831 Tsiatsiani, L., Van Breusegem, F., Gallois, P., Zavialov, A., Lam, E., and Bozhkov, P.: Metacaspases,
832 *Cell Death & Differentiation*, 18, 1279-1288, 2011.

833 Turk-Kubo, K. A., Frank, I. E., Hogan, M. E., Desnues, A., Bonnet, S., and Zehr, J. P.: Diazotroph
834 community succession during the VAHINE mesocosm experiment (New Caledonia lagoon),
835 *Biogeosciences*, 12, 7435-7452, 2015.

836 Urbani, R., Magaletti, E., Sist, P., and Cicero, A. M.: Extracellular carbohydrates released by the
837 marine diatoms *Cylindrotheca closterium*, *Thalassiosira pseudonana* and *Skeletonema costatum*:
838 Effect of P-depletion and growth status, *Science of the Total Environment*, 353, 300-306, 2005.

839 Vardi, A., Haramaty, L., Van Mooy, B. A., Fredricks, H. F., Kimmance, S. A., Larsen, A., and Bidle,
840 K. D.: Host–virus dynamics and subcellular controls of cell fate in a natural coccolithophore
841 population, *P. Natl. Acad. Sci.*, 109, 19327–19332, 2012.

842 Verdugo, P., and Santschi, P. H.: Polymer dynamics of DOC networks and gel formation in seawater,
843 *Deep Sea Research Part II: Topical Studies in Oceanography*, 57, 1486-1493, 2010.

844 Westberry, T. K., and Siegel, D. A.: Spatial and temporal distribution of *Trichodesmium* blooms in the
845 world’s oceans, *Global Biogeochem. Cycles*, 20, GB4016, doi:10.1029/2005GB002673, 2006.
846
847
848
849
850
851
852
853
854
855
856

857 **Figure legends**

858

859 **Figure 1-** Temporal dynamics of surface chlorophyll-a concentrations in the long duration (LD)
860 stations (a) LDA (b) LDB and (c) LDC station. Chlorophyll a was measured over 5 days at each
861 station (marked in gray). Satellite data of daily surface chlorophyll a (mg m^{-3}) around the long duration
862 stations of OUTPACE was used to predict changes in photosynthetic biomass before and after our
863 measurements at the station (marked as dashed lines). Satellite data movies are added as
864 supplementary data (Supplementary videos S1, S2, S3). Chlorophyll a profiles in (d) LDA (e) LDB
865 and (f) LDC. Measurements of Chl *a* were taken on days 1 (black dot), 3 (white triangle) and 5 (grey
866 square) at the LDB station at 5 depths between surface and 200 m depths.

867

868 **Figure 2- (a-d)** Microscopic images of *Trichodesmium* from LDA and LDB. Observations of poor cell
869 integrity were reported for collected samples, with filaments at various stages of degradation and
870 colony under possible stress. (e) Confocal and (d) processed IMARIS images of *Rhizosolenia-Richel*
871 *symbioses* (het-1) at 6m (75 % surface incidence). Green fluorescence indicates the chloroplast of the
872 diatoms, and red fluorescence are the *Richelia* filaments; Microscopic observations indicate that near
873 the surface *Rhizosolenia* populations were already showing signs of decay since the silicified cell-wall
874 frustules were broken and free filaments of *Richelia* were observed. Images by Andrea Caputo.

875

876 **Figure 3- PCD indices from LDA and LDB (a)** Caspase-like activity from LDA (pM hydrolyzed mg
877 $\text{protein}^{-1} \text{min}^{-1}$) assessed by cleavage of the canonical fluorogenic substrate, z-IETD-AFC. (b)
878 Metacaspase activity from LDA ($\text{pM hydrolyzed mg protein}^{-1} \text{min}^{-1}$) assessed by cleavage of the
879 canonical fluorogenic substrate, Ac-VRPR-AMC. (c) Relationship between caspase-like activity and
880 metacaspase activity from LDA ($r=0.7, n=15, p=0.005$). (d) Caspase-like activity rats in LDB station
881 ($\text{pM hydrolyzed mg protein}^{-1} \text{min}^{-1}$), (e) Metacaspase activity in LDB station ($\text{pmol hydrolyzed mg}$
882 $\text{protein}^{-1} \text{min}^{-1}$), (f) Relationship between caspase-like activity and metacaspase activity in LDB station
883 ($r=0.7, n=15, p=0.001$). Caspase-like and metacaspase activates at LDA and LDB stations were
884 measured on days: 1(black dot), 3 (white triangle) and 5 (grey square) between surface and 200 m.
885 Error bars represent ± 1 standard deviation ($n=3$).

886

887 **Figure 4- (a)** Depth profiles of TEP concentrations ($\mu\text{g GX L}^{-1}$) at LDB station. Measurements were
888 taken on days 1, 3 and 5 at the station at surface-200 m depths. (b) The relationships between the
889 concentration of transparent exopolymeric particles (TEP), ($\mu\text{g GX L}^{-1}$) and dissolved inorganic
890 phosphorus DIP ($\mu\text{mol L}^{-1}$) for days 1, 3 and 5 at the LDB station ($r=-0.7, n=15, p=0.005$).
891 Relationships between the concentration of transparent exopolymeric particles (TEP), ($\mu\text{g GX L}^{-1}$) and
892 (c) metacaspase activity ($\text{pmol hydrolyzed mg protein}^{-1} \text{min}^{-1}$) for days 1, 3 and 5 at the LDB assessed
893 by cleavage of the canonical fluorogenic substrate, Ac-VRPR-AMC ($r =0.6 n=15, p=0.03$); (d) and

894 with dissolved organic carbon (DOC), (μM) for days 1, 3 and 5 at the LDB station ($r=0.7$, $n=15$,
895 $p=0.004$) (e) and with particulate organic carbon (POC) (μM) for days 1, 3 and 5 at the LDB station
896 ($r=0.8$, $n=5$, $p=0.1$ for day 1 and $r=0.9$, $n=8$ $p=0.002$ for day 3 and 5) (f) and with total organic carbon
897 (TOC) (μM) for days 1, 3 and 5 at the LDB station ($r=0.7$, $n=15$, $p=0.001$). Measurements were taken
898 on days 1 (black dot), 3 (white triangle) and 5 (grey square) at LDB at 5 depths between surface and
899 200 m depths. Error bars for TEP represent ± 1 standard deviation ($n=3$).

900

901 **Figure 5-** (a) Diazotrophic abundance (*nifH* copies L^{-1}) of *Trichodesmium* (dark grey bars); UCYN-B
902 (white bars); and het-1 (light grey bars) recovered in sediment traps at the long duration stations (A)
903 Diazotrophic abundance (*nifH* copies L^{-1}) observed in the traps at LDA station (b) Diazotrophic
904 abundance (*nifH* copies L^{-1}) observed in the traps at LDB station. Abundance was measured from the
905 accumulated material on day 5 at each station. Sediment traps were deployed at the LD station at 150
906 m, 325 m, and 500 m. Error bars represent ± 1 standard deviation ($n=3$). (c) Relationship between
907 metacaspase activity ($\text{pmol hydrolyzed mg protein}^{-1} \text{ min}^{-1}$) measured at the surface waters of LDA
908 station assessed by cleavage of the canonical fluorogenic substrate, Ac-VRPR-AMC and mass flux
909 rates ($\text{mg m}^2 \text{ h}^{-1}$) (green circle), particulate carbon (PC, mg sample^{-1}) (green triangle) and particulate
910 nitrogen (PN, mg sample^{-1}) (green square) measured in the sediment trap deployed at 150 m. A 1-day
911 shift between metacaspase activities at the surface showed a significant positive correlation with mass
912 flux and particulate matter obtained in the sediment trap at LDA station at 150 m.

913

914

915

916

917

918

919

920

921

922

923

924

925

926

927 **Table 1-** Temporal changes in the relative composition (w/w) and distribution of TEP, TEP-C and
 928 organic carbon and nitrogen fractions within the water column during days 1,3 and 5 in the LDA
 929 station at different depth ranging between surface (10 m) to 200 m.
 930

Day at LDA station	Depth (m)	TEP ($\mu\text{g GX L}^{-1}$)	TEP-C	%TEP-C	POC (μM)	TOC (μM)	POC/PON
1	200	296 \pm 135	186.5	27.2	3.04	57.2	5
	150	ND	ND	ND	3.18	61.1	13
	70	87 \pm 17	54.8	6.7	2.93	68.7	11
	50	562 \pm 7	354.3	41.9	2.47	70.5	13
	10	241 \pm 40	152.3	14.5	9.21	87.4	8
3	200	191 \pm 13	120.9	18.6	1.29	54.2	27
	150	144 \pm 54	91.2	12.9	2.22	59.0	22
	80	263	166.1	20.5	4.62	67.5	15
	10	126 \pm 2	79.6	8.3	3.60	79.7	12
5	200	200	126	21.3	2.84	54.2	236
	150	220	138.6	18.0	2.72	58.2	7
	80	146	92.2	12.1	4.91	63.3	8
	50	348 \pm 60	219.5	26.8	3.33	68.3	6
	10	ND	ND	ND	5.80	83.7	7

931
 932
 933
 934
 935
 936
 937

Table 2- Temporal changes in the relative composition (w/w) and distribution of TEP, TEP-C and organic carbon and nitrogen fractions within the water column during days 1,3 and 5 in the LDB station at different depth ranging between surface (7 m) to 200 m.

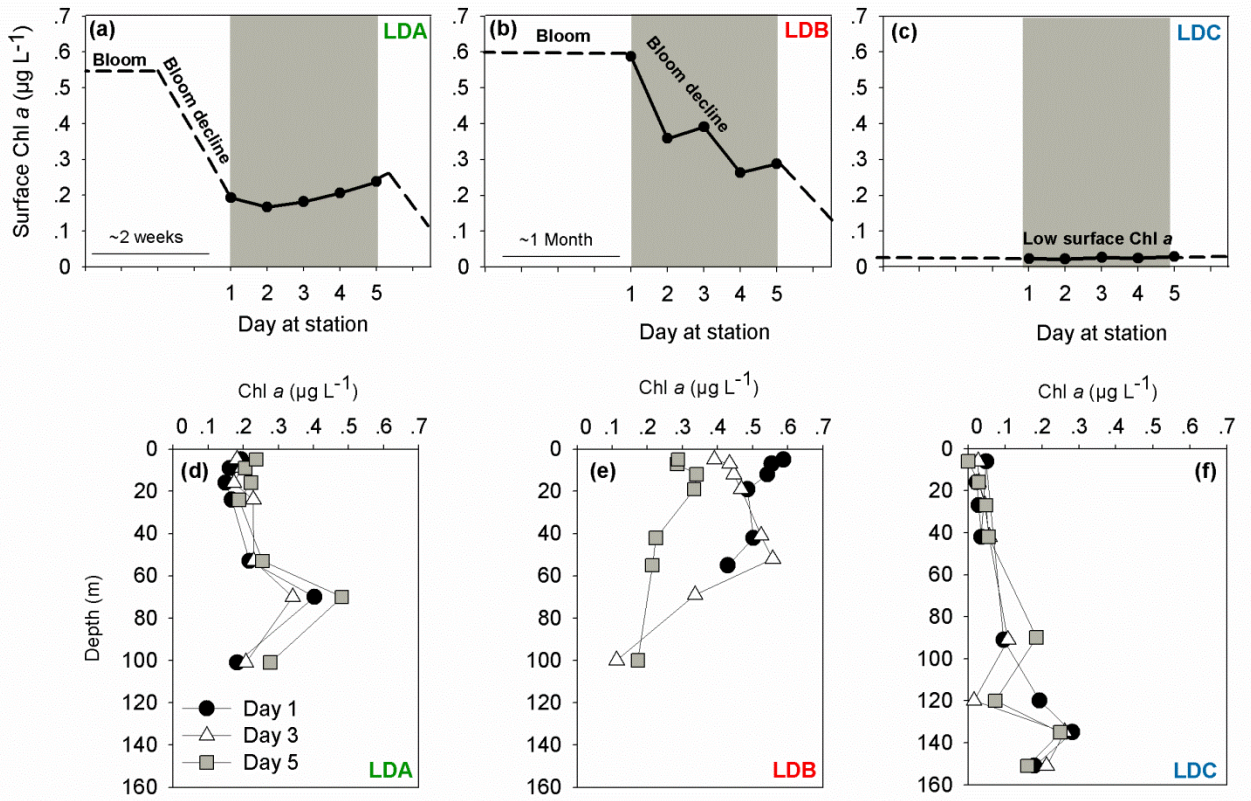
Day at LDB station	Depth (m)	TEP ($\mu\text{g GX L}^{-1}$)	TEP-C	%TEP-C	POC (μM)	TOC (μM)	POC/PON
1	7	408 \pm 36	257.1	23.4	8.95	91.5	6.0
	35	279 \pm 86	175.9	17.0	5.86	86.0	9.1
	100	214 \pm 67	134.7	16.8	ND	66.7	ND
	150	145 \pm 34	91.5	12.3	3.79	61.9	11.2
	200	244 \pm 113	153.7	20.3	7.61	63.2	9.8
3	7	402 \pm 12	253.1	22.5	8.88	93.9	6.9
	35	193 \pm 48	121.8	12.6	3.07	80.3	8.2
	100	163 \pm 33	102.4	12.6	ND	67.8	ND
	150	145 \pm 34	91.6	12.0	1.91	63.8	7.4
	200	127 \pm 79	80.2	11.3	1.71	59.3	5.7
5	7	565 \pm 87	355.8	32.5	5.32	91.3	5.9
	70	294 \pm 53	185.2	20.1	2.21	76.7	6.1
	100	264 \pm 160	166.2	19.6	2.25	70.6	8.0
	150	224 \pm 51	140.8	15.9	1.53	73.9	5.1
	200	231 \pm 45	145.8	21.1	1.11	57.6	5.5

938
 939 Abbreviations: TEP, transparent exopolymeric particle; TEP-C, TEP carbon; POC, particulate organic
 940 C; TOC, total organic C; ND- no data.
 941

942

943 **Figures**

944 **Figure 1**



945

946

947

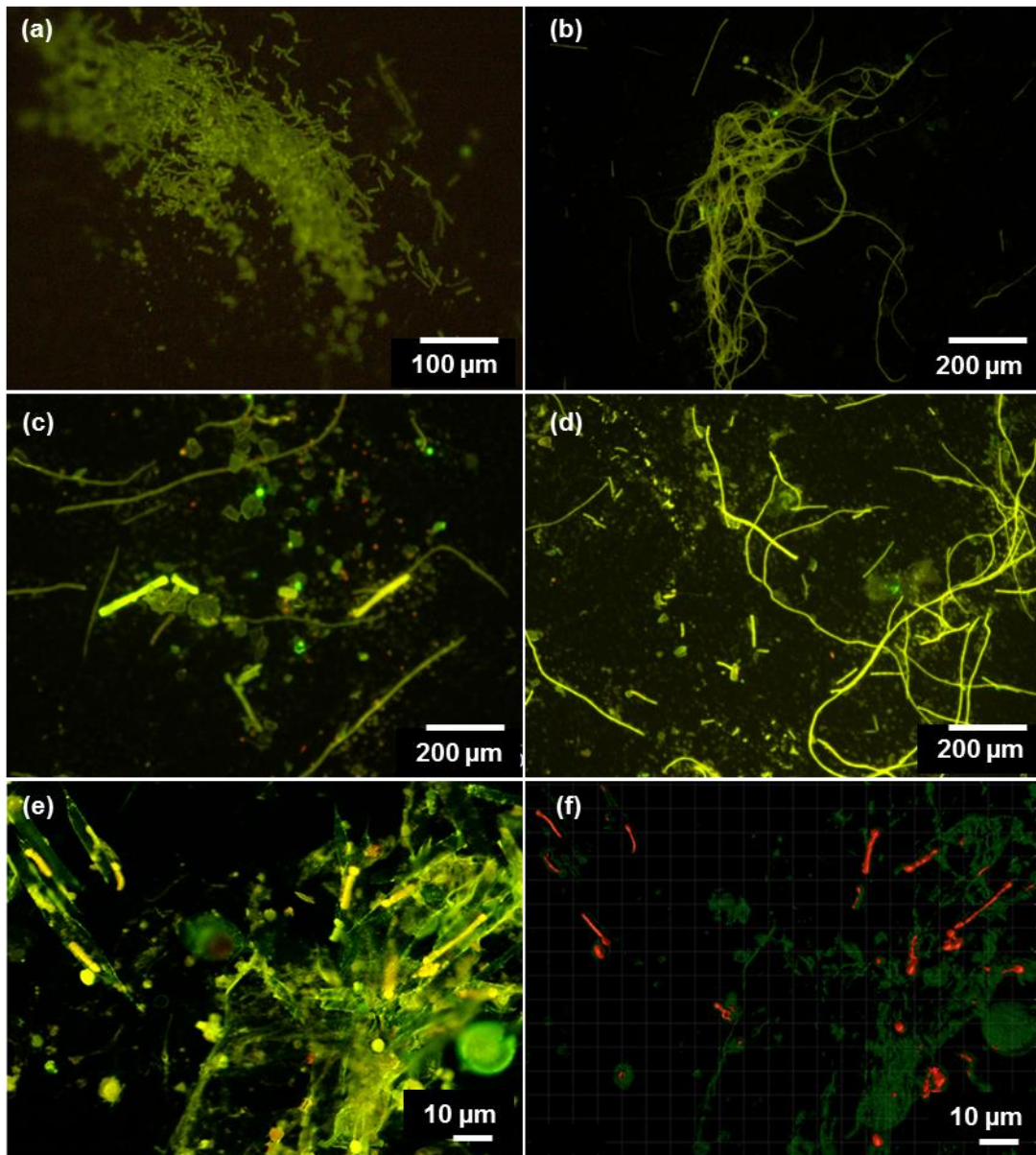
948

949

950

951

952 **Figure 2**



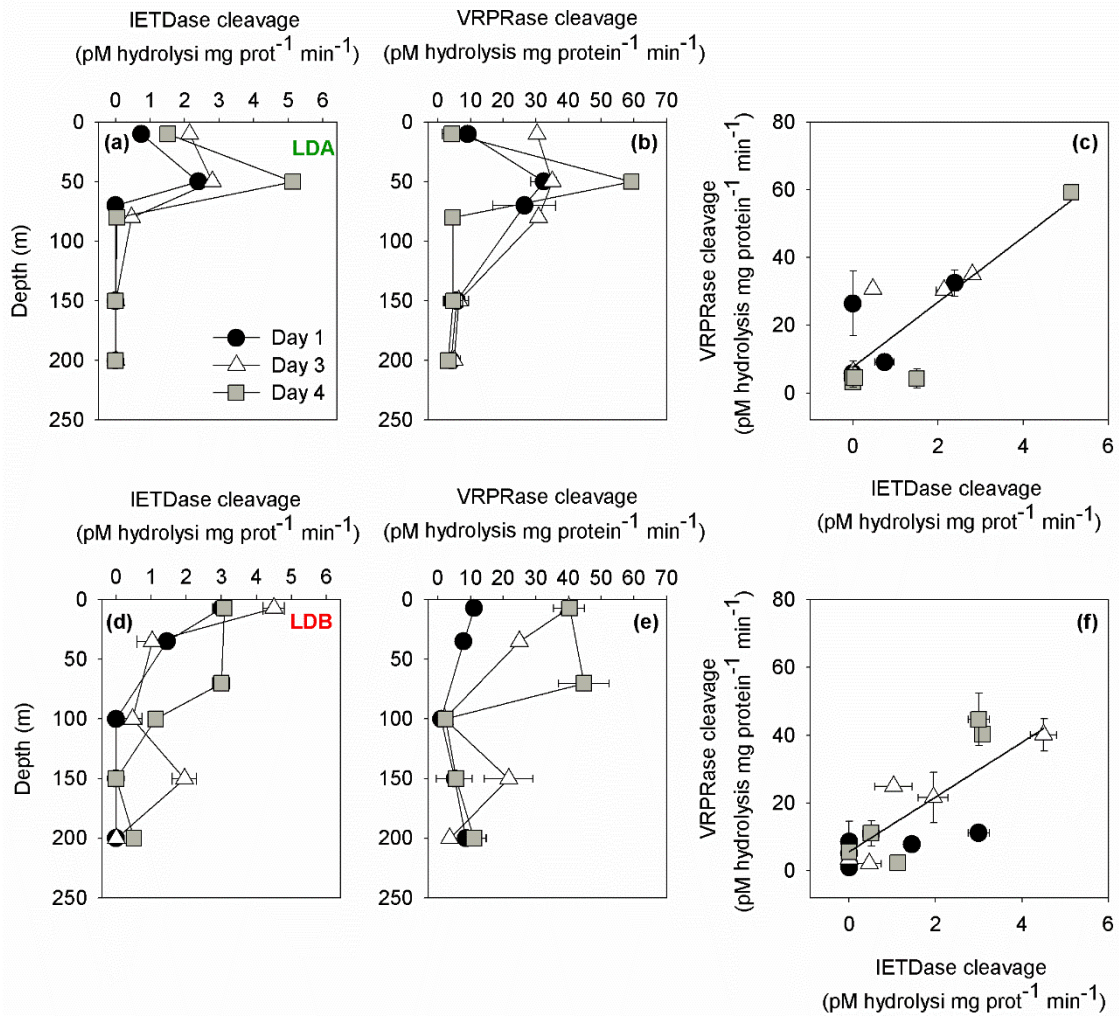
953

954

955

956

957



959

960

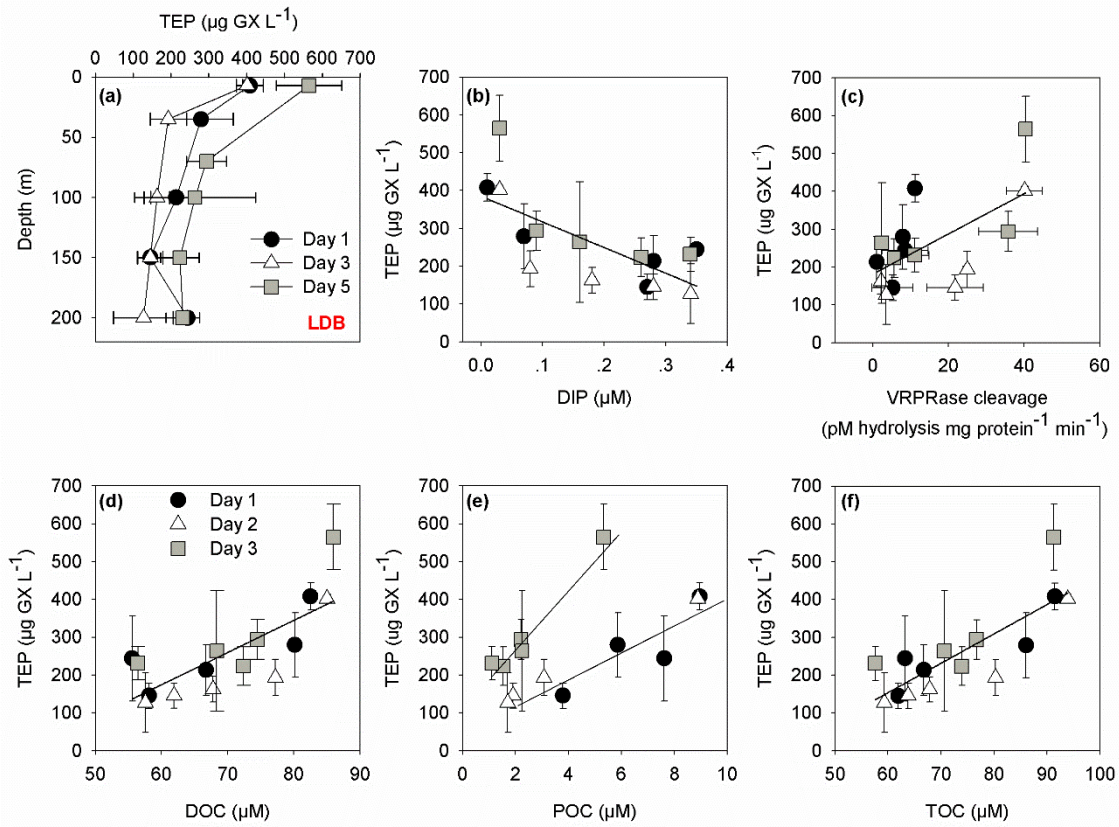
961

962

963

964

965



967

968

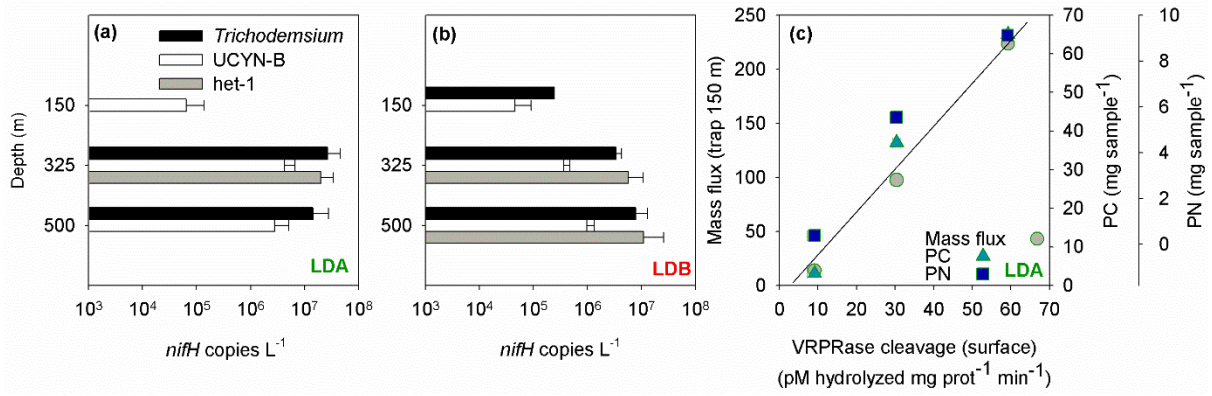
969

970

971

972

973 **Figure 5**



974

975